# Synthesis and Characterization of a Series of Triethylphosphine-Ligated Pt−Au Cluster Compounds. X-ray Crystal and Molecular Structure of $[Pt(AuPEt_3)_9](NO_3)_3$

**Don A. Krogstad, Wayde V. Konze, and Louis H. Pignolet***

Department of Chemistry, University of Minnesota, Minneapolis, Minnesota 55455

*Received May 22, 1996*[⊗]

The first triethylphosphine-stabilized Pt−Au cluster compounds, $[Pt(AuPEt_3)_{10}]^{2+}$ (**2**) and $[Pt(AuPEt_3)_9]^{3+}$ (**3**), were prepared by the direct reaction of $Pt(PEt_3)_3$ with $AuPEt_3NO_3$ under a dihydrogen atmosphere. Cluster **2** is the highest-nuclearity homoleptic $Pt(AuPR_3)_n$ cluster yet prepared. The reactivity and structures of these clusters are in agreement with the well-established electron-counting arguments. The 18-electron cluster **2** was converted into the 16-electron cluster **3** by *oxidation* with 2 equiv of ferricinium ion $[Fe(\eta^5\text{-}C_5H_5)_2]^+$. Cluster **3** was converted into **2** by *reduction* with $H_2$ in the presence of $[AuPEt_3]^+$. Cluster **3** was also observed to cleanly add the 2-electron donors CO and $PEt_3$ to form the 18-electron clusters $[(CO)Pt(AuPEt_3)_9]^{3+}$ (**4**) and $[(PEt_3)Pt(AuPEt_3)_9]^{3+}$ (**5**), respectively. Single-crystal X-ray diffraction results show that **3** has a flattened, toroidal structure in which the $PtAu_9$ framework has a Pt-centered, tricapped trigonal prismatic geometry. Crystal data for $[Pt(AuPEt_3)_9](NO_3)_3$ is as follows: hexagonal $P6_3/m$, $a = 15.134(5)$ Å, $c = 23.48(1)$ Å, $V = 4657$ Å$^3$, $Z = 2$, residuals $R = 0.056$, and $R_w = 0.053$ for 1489 observed reflections and 81 variables, Mo Kα radiation. Compound **3** was found to reversibly add $H_2$ in solution to form the dihydride cluster $[(H)_2Pt(AuPEt_3)_9]^{3+}$ (**6**). The equilibrium constant for this addition reaction is $1.1 \times 10^3$ M$^{-1}$ ($CD_2Cl_2$ solution, 25 °C), slightly smaller than that for $[Pt(AuPPh_3)_8]^{2+}$. The rate of the addition is also slower than that with $[Pt(AuPPh_3)_8]^{2+}$. Cluster **3** is an excellent homogeneous catalyst for $H_2-D_2$ equilibration giving a turnover rate for HD production of 0.13 s$^{-1}$ (nitrobenzene solvent, 30 °C, 1 atm). The $PEt_3$-containing clusters give similar rates and follow the same general trends previously observed with $PPh_3$-ligated clusters. The chemistry of these new clusters is explained by consideration of the steric and electronic properties of the $PEt_3$ ligand. These new compounds will be useful as models for hydrogen activation by Pt−Au clusters and as precursors for supported Pt−Au catalysts.

## Introduction

A large number of $PR_3$-stabilized, Pt−Au cluster compounds have been prepared and characterized during the past decade.[1−8] $[Pt(AuPPh_3)_8](NO_3)_2$ has received the most attention because of its extensive reaction chemistry including its surprising ability to reversibly bind and activate $H_2$.[1,9,10] The vast majority of Pt−Au cluster compounds studied are ligated with $PPh_3$. We are unaware of any examples with trialkylphosphine ligands. We therefore initiated a project to prepare a series of Pt−Au clusters that are ligated exclusively with $PEt_3$. The objectives of this project were to examine the steric and electronic effects on cluster formation, structure, and reactivity. We considered this project especially relevant due to the recent use of Pt−Au clusters as $H_2$ activation catalysts. For example, $[Pt(AuPPh_3)_8]^{2+}$ and related $PPh_3$-ligated clusters are excellent catalysts for $H_2-D_2$ equilibration ($H_2 + D_2 \rightleftarrows 2HD$) in homogeneous solution phase and in the solid state.[1,9−12] They were also found to catalyze $D_2(g)-H_2O(l)$ isotope exchange in homogeneous pyridine solution.[13] These catalytic reactions have proven useful as probes of structure−reactivity relations for a number of heterometallic clusters.[1,10] The $H_2-D_2$ equilibration reaction has also been used to probe the nature of Pt−Au clusters on silica and alumina supports.[12,14] Considerable effort is being devoted to studying the mechanism of these isotope exchange reactions, and the availability of clusters with different ligands and structures will be very useful.[15] Hydrogen activation is of fundamental importance in the area of catalysis, and few studies of this process have been carried out with heterometallic cluster compounds.

The bonding in $[Pt(AuPPR_3)_n]^{x+}$ clusters has been described in terms of the interactions between radially hybridized (s−z) orbitals in the $AuPR_3$ fragments. The following closed shell requirements have been derived from extended Hückel molecular orbital calculations and the tensor surface harmonic theory.[2,16−18] Clusters with 16 valence electrons, $(S^\sigma)^2(P^\sigma)^4$ plus the 10 electrons in the d shell of the central Pt, should have a

[⊗] Abstract published in *Advance ACS Abstracts,* October 15, 1996.

(1) Pignolet, L. H.; Aubart, M. A.; Craighead, K. L.; Gould, R. A. T.; Krogstad, D. A.; Wiley, J. S. *Coord. Chem. Rev.* **1995**, *143*, 219.
(2) Mingos, D. M. P.; Watson, M. J. *Adv. Inorg. Chem.* **1992**, *39*, 327.
(3) Steggerda, J. J. *Comments Inorg. Chem.* **1991**, *11*, 113.
(4) Mueting, A. M.; Bos, W.; Alexander, B. D.; Boyle, P. D.; Casalnuovo, J. A.; Balaban, S.; Ito, L. N.; Johnson, S. M.; Pignolet, L. H. *New J. Chem.* **1988**, *12*, 505.
(5) Teo, B. K.; Zhang, H. *Coord. Chem. Rev.* **1995**, *143*, 611.
(6) Kappen, T. G. M. M.; Schlebos, P. P. J.; Bour, J. J.; Bosman, W. P.; Beurskens, G.; Smits, J. M. M.; Beurskens, P. T.; Steggerda, J. J. *Inorg. Chem.* **1995**, *34*, 2121.
(7) Kappen, T. G. M. M.; Schlebos, P. P. J.; Bour, J. J.; Bosman, W. P.; Smits, J. M. M.; Beurskens, P. T.; Steggerda, J. J. *Inorg. Chem.* **1995**, *34*, 2133.
(8) Gould, R. A. T.; Craighead, K. L.; Wiley, J. S.; Pignolet, L. H. *Inorg. Chem.* **1995**, *34*, 2902.
(9) Kappen, T. G. M. M.; Bour, J. J.; Schlebos, P. P. J.; Roelofsen, A. M.; van der Linden, J. G. M.; Steggerda, J. J.; Aubart, M. A.; Krogstad, D. A.; Schoondergang, M. F. J.; Pignolet, L. H. *Inorg. Chem.* **1993**, *32*, 1074.
(10) Aubart, M. A.; Chandler, B. D.; Gould, R. A. T.; Krogstad, D. A.; Schoondergang, M. F. J.; Pignolet, L. H. *Inorg. Chem.* **1994**, *33*, 3724.
(11) Aubart, M. A.; Pignolet, L. H. *J. Am. Chem. Soc.* **1992**, *114*, 7901.
(12) Graf, I. V. G.; Bacon, J. W.; Consugar, M. B.; Curley, M. E.; Ito, L. N.; Pignolet, L. H. *Inorg. Chem.* **1996**, *35*, 689.
(13) Aubart, M. A.; Koch, J. F. D.; Pignolet, L. H. *Inorg. Chem.* **1994**, *33*, 3852.
(14) Yuan, Y.; Asakura, K.; Wan, H.; Tsai, K.; Iwasawa, Y. *Chem. Lett.* **1996**, 129.
(15) Rubinstein, L. I.; Pignolet, L. H. *Inorg. Chem.* **1996**, *35*, in press.
(16) Stone, A. J. *Inorg. Chem.* **1981**, *20*, 563.
(17) Mingos, D. M. P.; Johnson, R. J. *Struct. Bonding* (*Berlin*) **1987**, *68*, 29.

S0020-1669(96)00586-1 CCC: $12.00 

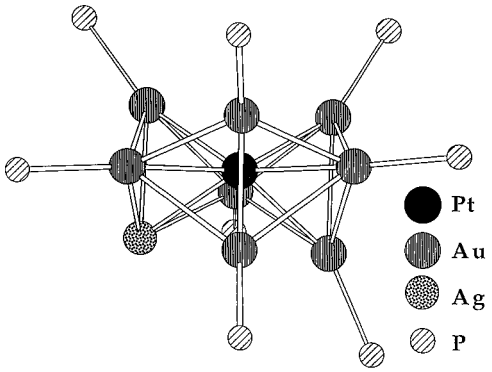


**Figure 1.** Structure of the $PtAu_8Ag$ core of the 16-electron cluster $[(AgNO_3)Pt(AuPPh_3)_8]^{2+}$ illustrating the toroidal geomtrey. Drawn from the positional parameters given in ref 19.

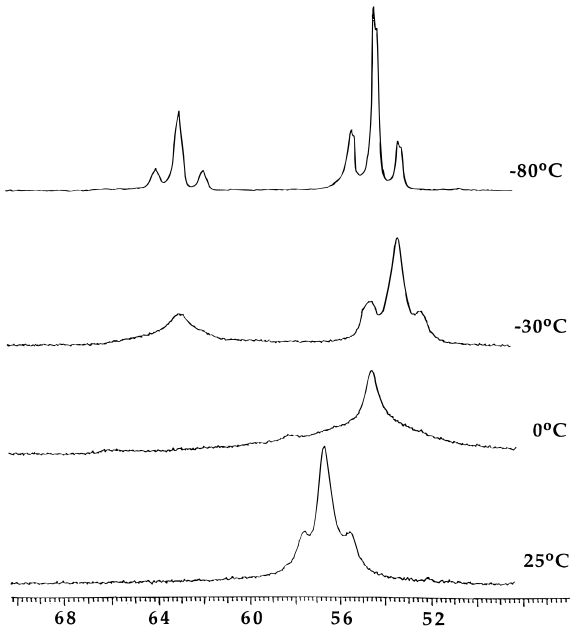


**Figure 2.** $^{31}P\{^1H\}$ NMR spectra of $[Pt(AuPEt_3)_9]^{3+}$ **(3)** recorded at various temperatures (202.5 MHz with $CD_2Cl_2$ as solvent).

toroidal or elliptical arrangement of the Au atoms, while in 18-electron clusters, $(S^\sigma)^2(P^\sigma)^6$ plus 10, the Au atoms should lie approximately in a spherical arrangement. These structural predictions have been confirmed experimentally.[1−3,17,18] An example relevant to the present study is the 16-electron, trimetallic cluster $[(AgNO_3)Pt(AuPPh_3)_8]^{2+}$ whose structure is shown in Figure 1.[19] The toroidal structure of this cluster is clearly evident. Reactivity patterns have also been rationalized by this electron-counting formalism.[1−3] Thus, 16-electron clusters typically add 2-electron donor ligands such as CO to form complete shell, 18-electron adducts. The 18-electron clusters do not add 2-electron donor ligands, but may add metallic electrophiles such as $AgNO_3$ or CuCl if the steric demand of the cluster permits.

In this paper we report the preparation and characterization of a new series of $[Pt(AuPEt_3)_n]^{x+}$ clusters and examine their reactions with $H_2$, CO, $PEt_3$, $AgNO_3$, and CuCl, their redox properties, and $H_2$ activation catalysis chemistry. While the results are in general agreement with the above electron-counting formalism, the clusters formed are more reactive and of higher nuclearity than their $PPh_3$ analogs. The cluster $[Pt(AuPEt_3)_{10}]^{2+}$ is the highest-nuclearity homoleptic $Pt(AuPR_3)_n$ cluster yet prepared. The chemistry of these clusters is explained by consideration of the steric and electronic properties of the $PEt_3$ ligand.

**Scheme 1**

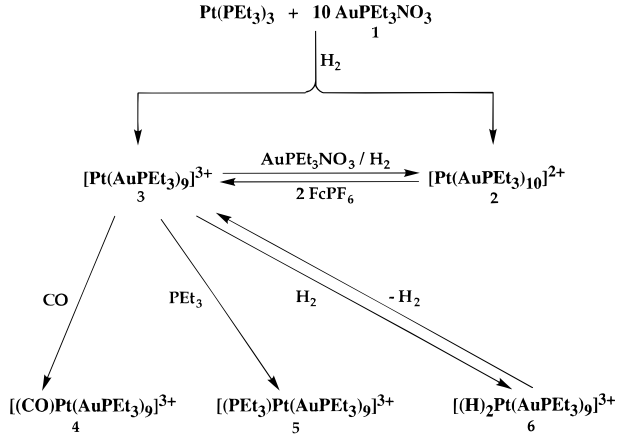


## Results

**Synthesis and Characterization.** The reactions observed in this study are summarized in Scheme 1 and described in the Experimental Section. Characterization data for compounds **1**−**6** are included in the Experimental Section and, when appropriate, discussed below. Under a hydrogen atmosphere, reaction of $Pt(PEt_3)_3$ with 10 equiv of $AuPEt_3NO_3$ **(1)** in THF produced a mixture of $[Pt(AuPEt_3)_{10}]^{2+}$ **(2)** and $[Pt(AuPEt_3)_9]^{3+}$ **(3)**. Both clusters were cleanly separated and isolated as $PF_6$ salts due to differences in solubility. When the reaction was performed in EtOH solution, however, $\mathbf{3(PF_6)_3}$ precipitated in high yield from the reaction without any evidence of $\mathbf{2(PF_6)_2}$ formation. Both clusters have been characterized by $^{31}P\{^1H\}$ and $^1H$ NMR and IR spectroscopies FABMS, and elemental analysis.

The temperature dependence of the $^{31}P\{^1H\}$ NMR spectrum of **3** is shown in Figure 2. At room temperature, a broad triplet pattern at 57.0 ppm is observed, suggesting a fast to intermediate exchange between distinct P sites. Lowering of the temperature caused the resonance to broaden and decoalesce into two pseudo-triplets at approximately 53.5 and 63.0 ppm. At −80 °C, these peaks sharpened into two distinct phosphorus signals centered at 55.8 and 63.0 ppm in a 2:1 intensity ratio, respectively. Coupling due to $^{195}Pt$ caused the pseudo-triplet patterns. It is well-known that phosphine-stabilized M−Au clusters can exist as a mixture of structural isomers that rapidly interconvert in solution.[15] Therefore, the low-temperature spectrum of Figure 2 could be the result of two different isomers of **3** or, alternatively, two nonequivalent phosphorus environments within one structural form. To clarify this issue, a double-quantum filtered, proton decoupled phase sensitive COSY $^{31}P$ NMR experiment was performed at −80 °C. This two-dimensional spectrum is shown in Figure 3. Figure 3 clearly indicates that the $\delta = 55.8$ ppm resonance and its $^{195}Pt$ satellites couple with the $\delta = 63.0$ ppm resonance and its satellites. Therefore, the low-temperature spectrum of Figure 2 is the result of two distinct phosphorus environments in the same molecule. The $^{31}P$ NMR splitting pattern and intensities are in complete agreement with the X-ray structure of **3** (vide infra). The dynamic process that averages these environments as the temperature increases is well established in M−Au cluster

(18) Mingos, D. M. P.; Wales, D. J. *Review of Cluster Chemistry*; Englewood Cliffs, NJ, 1990.
(19) Kanters, R. P. F.; Schlebos, P. P. J.; Bour, J. J.; Bosman, W. P.; Smits, J. M. M.; Beurskens, P. T.; Steggerda, J. J. *Inorg. Chem.* **1990**, *29*, 324.

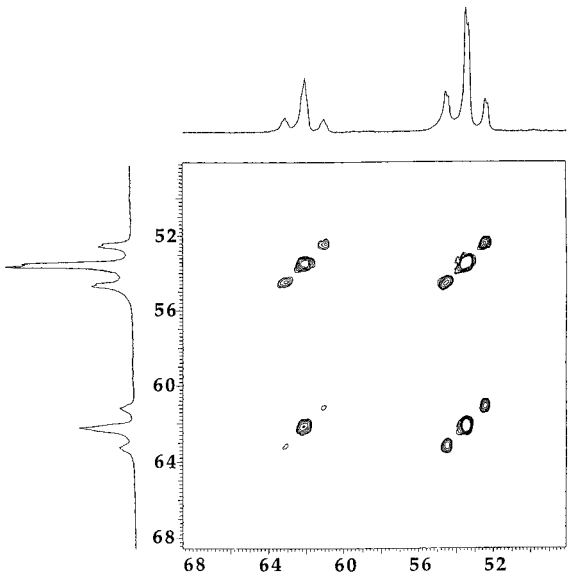


**Figure 3.** Double-quantum filtered $^{31}P\{^1H\}$ NMR phase sensitive COSY spectrum of $[Pt(AuPEt_3)_9]^{3+}$ **(3)** at −80 °C (202.5 MHz with $CD_2Cl_2$ as solvent).

chemistry and results from rapid skeletal rearrangement of $AuPR_3$ units.[1−3,20]

Using the electron counting rules for M−Au clusters described above, $[Pt(AuPEt_3)_{10}]^{2+}$ **(2)** and $[Pt(AuPEt_3)_9]^{3+}$ **(3)** are classified as 18- and 16-electron clusters, respectively. The reactivity of **2** and **3** is in agreement with this electron-counting formalism. Cluster **2** was converted into **3** by *oxidation* with ferricinium ion, $Fc^+$, and **3** converted into **2** by *reduction* with $H_2$ in the presence of $[AuPEt_3]^+$. The 16-electron cluster **3** also reacted cleanly with the 2-electron donors CO and $PEt_3$ to form the 18-electron clusters $[(CO)Pt(AuPEt_3)_9]^{3+}$ **(4)** and $[(PEt_3)Pt(AuPEt_3)_9]^{3+}$ **(5)**, respectively, while **2** was unreactive toward these ligands. The clusters **4** and **5** were prepared in excellent yield and characterized by standard spectroscopic and analytical techniques. The carbonyl stretching frequency of **4** ($\nu$(CO) = 1948 $cm^{-1}$) is 8 $cm^{-1}$ higher than that of $[(CO)Pt(AuPPh_3)_8]^{2+}$.[21] This suggests that even though $PEt_3$ is a more basic phosphine, the electron density of the Pt center is lower. This is probably due to the greater positive charge on **3**. The formation of **5** is of interest because it is prepared by the direct addition of $PEt_3$ to the Pt center. The addition of a $PR_3$ ligand to the Pt of a 16-electron Pt−Au cluster has not been observed with $PPh_3$. This observed reactivity difference is probably due to the greater basicity and smaller size of $PEt_3$ compared to $PPh_3$.

Reactions of **2** and **3** were also attempted with the electrophiles M′X (M′X = $AgNO_3$ and CuCl. These reagents are known to add cleanly to $[Pt(AuPPh_3)_8]^{2+}$ and $[(CO)Pt(AuPPh_3)_8]^{2+}$ in solution giving the adducts $[(M'X)Pt(AuPPh_3)_8]^{2+}$ and $[(M'X)(CO)Pt(AuPPh_3)_8]^{2+}$.[19,22] No reaction was observed with the 18-electron cluster **2**, and more surprisingly, decomposition occurred with **3**. Cluster **3** did react reversibly with $H_2$ in solution to form the 18-electron, dihydride $[(H)_2Pt(AuPEt_3)_9]^{3+}$ **(6)**. The equilibrium constant for this reaction was determined and is $1.1 \times 10^3$ $M^{-1}$ at 30 °C in $CD_2Cl_2$ solution (vide infra). An analogous reversible reaction is known with $[Pt(AuPPh_3)_8]^{2+}$ to give $[(H)_2Pt(AuPPh_3)_8]^{2+}$.[1,9,10] These reactions will be discussed below.

(20) Salter, I. D. *Adv. Organomet. Chem.* **1989**, *29*, 249.
(21) Kanters, R. P. F.; Schlebos, P. P. J.; Bour, J. J.; Bosman, W. P.; Behm, H. J.; Steggerda, J. J. *Inorg. Chem.* **1988**, *27*, 4034.
(22) Schoondergang, M. F. J.; Bour, J. J.; Schlebos, P. P. J.; Vermeer, A. W. P.; Bosman, W. P.; Smits, J. M. M.; Beurskens, P. T.; Steggerda, J. J. *Inorg. Chem.* **1991**, *30*, 4704.

**Table 1.** Crystallographic Data for $[Pt(AuPEt_3)_9](PF_6)_3$ **($3(PF_6)_3$)**

| | |
|---|---|
| Crystal Parameters and Measurement of Intensity Data | |
| cryst syst | hexagonal |
| space group | $P6_3/m$ (No. 176) |
| cryst dimens | 0.420 × 0.420 × 0.310 |
| cell parameters at *T*, °C | +24 |
| *a*, Å | 15.134(5) |
| *c*, Å | 23.48(1) |
| *V*, Å$^3$ | 4657(6) |
| *Z* | 2 |
| calcd density, g $cm^{-3}$ | 2.483 |
| abs coeff, $cm^{-1}$ | 158.57 |
| max, min transm factors | 0.72, 1.52 |
| formula | $C_{54}H_{135}F_{18}P_{12}Au_9Pt$ |
| fw, amu | 3482.10 |
| diffractometer | Enraf-Nonius CAD-4 |
| radiation | Mo Kα ($\lambda$ = 0.71069 Å) |
| scan type; range ($2\theta$), deg | $\omega$ scan, 0−48 |
| no. of unique rflcns measd | 2523 |
| no. of obsd rflcns | 1489 [$I > 2.0\sigma(I)$] |
| Refinement by Full-Matrix Least Squares | |
| no. of variables | 81 |
| $R^a$ | 0.056 |
| $R_w{}^a$ | 0.053 |
| goodness of fit$^a$ | 1.28 |
| *p*-factor | 0.03 |

$^a$ The function minimized was $\sum w(|F_o| - |F_c|)^2$, where $w = 4F_o{}^2/s^2(F_o{}^2)$ and $\sigma^2(F_o{}^2) = [S^2(C + R^2 + B) + (pF_o{}^2)^2]/Lp^2$, $S$ = scan rate, $C$ = total integrated peak count, $R$ = ratio of scan time to background counting time, B = total background count, Lp = Lorentz-polarization factor, and $p$ = $p$-factor used to downweight intense reflections. The unweighted and weighted residuals are defined as $R = \sum(||F_o| - |F_c||)/\sum|F_o|$ and $R_w = [(\sum w(|F_o| - |F_c|)^2)/(\sum w|F_o|^2)]^{1/2}$. The error in an observation of unit weight (GOF) is $[\sum w(|F_o| - |F_c|)^2/(N_o - N_v)]^{1/2}$, where $N_o$ and $N_v$ are the number of observations and variables, respectively.

**Table 2.** Selected Bond Lengths (Å) and Angles (deg) with Esd's for the Cluster Core of $[Pt(AuPEt_3)_9](PF_6)_3$ **($3(PF_6)_3$)**$^a$

| | | | |
|---|---|---|---|
| Bond Lengths | | | |
| Pt−Au1 | 2.680(2) | Au1−P1 | 2.29(1) |
| Pt−Au2 | 2.725(1) | Au2−P2 | 2.303(7) |
| Au1−Au2 | 2.893(2) | Au2−Au2* | 2.752(2) |
| Au1−Au2* | 2.870(2) | | |
| Bond Angles | | | |
| Au1−Pt−Au1′ | 120.0(0) | Pt−Au1−P1 | 178.9(3) |
| Au1−Pt−Au2 | 64.72(3) | Pt−Au2−P2 | 156.9(2) |
| Au1−Pt−Au2′ | 64.15(4) | Au2−Pt−Au2′ | 96.74(3) |
| Au1−Pt−Au2″ | 149.66(3) | Au2−Pt−Au2*′ | 128.87(1) |
| | | Au2−Pt−Au2* | 60.67(5) |

$^a$ See Figure 4 for a definition of the atom labels.

**Crystal Structure of $[Pt(AuPEt_3)_9](PF_6)_3$ ($3(PF_6)_3$).** A summary of crystal data is presented in Table 1. Selected positional and thermal parameters and interatomic distances and angles are listed in Tables 2 and 3, respectively. The geometry of the metal core and numbering scheme are presented in Figure 4. Additional crystallographic data are provided as Supporting Information.

The cluster cation is on a $\bar{6}$ position and therefore has $C_{3h}$ point group symmetry. There is a crystallographic mirror plane containing the atoms Au1, Au1′, Au1″, and Pt and a $C_3$ rotation axis perpendicular to this plane through Pt. The geometry of the $PtAu_9$ framework is that of a centered, tricapped trigonal prism with approximate $D_{3h}$ symmetry. The ethyl groups of the ligands prevent the molecule from having perfect $D_{3h}$ symmetry. This is a classic structure for nine-coordinate systems[23] and causes the three P1 phosphorus atoms to be nonequivalent to the six P2 phosphorus atoms. This nonequiva-

(23) Favas, M. C.; Kepert, D. L. *Prog. Inorg. Chem.* **1981**, *28*, 309.

**Table 3.** Comparison of Selected Bond Distances (Å) and Angles (deg) in M−$PtAu_8$ Cluster Compounds (M = Au, Ag, Cu)[a]

| | $[Pt(AuPEt_3)_9](PF_6)_3$ **(3)** | $[(AgNO_3)Pt(AuPPh_3)_8](NO_3)_2$ | $[(CuCl)Pt(AuPPh_3)_8](NO_3)_2$ |
|---|---|---|---|
| Pt−Au (all) | 2.710 (2.680, 2.725) | 2.650 (2.634−2.684) | 2.673 (2.640−2.694) |
| Pt−Au (middle)[b] | 2.680 | 2.649 (2.607−2.682) | 2.690 (2.684−2.692) |
| Pt−Au (outer)[b] | 2.725 | 2.650 (2.608−2.684) | 2.663 (2.640−2.681) |
| Au−Au (all)[c] | 2.856 (2.752, 2.882) | 2.850 (2.726−3.042) | 2.881 (2.779−3.112) |
| P−Au | 2.30 (2.29, 2.30) | 2.27 (2.20−2.30) | 2.29 (2.27−2.32) |
| P−Au (middle)[b] | 2.29 | 2.26 (2.20−2.30) | 2.31 (2.29−2.32) |
| P−Au (outer)[b] | 2.30 | 2.27 (2.22−2.30) | 2.28 (2.27−2.29) |
| Pt−Au−P (all) | 164.3 (156.9, 178.9) | 163.2 (151.4−173.7) | 163.0 (148.7−174.3) |
| Pt−Au−P (middle)[b] | 178.9 | 171.8 (169.1−173.7) | 173.1 (171.4−174.3) |
| Pt−Au−P (outer)[b] | 156.9 | 158.0 (151.4−162.4) | 156.9 (148.7−166.1) |

[a] Distances and angles are given as average values, and ranges are in parentheses. [b] The middle Au atoms of **3** are Au1, Au1′, Au1″ and lie in the mirror plane; the six Au2 atoms are defined as outer. An analogous definition follows for the Ag and Cu trimetallic clusters, see Figure 4. [c] Au−Au distances are for adjacent, bonded Au atoms only. These are shown by solid lines in Figure 4.

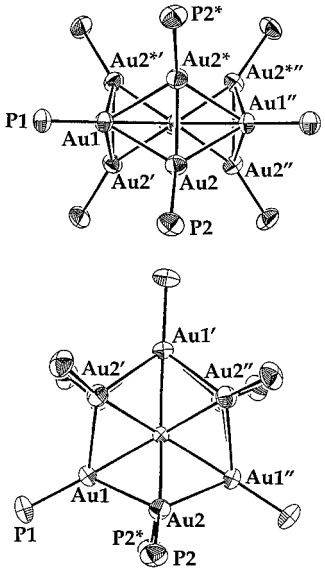


**Figure 4.** ORTEP representations of the cluster core of $[Pt(AuPEt_3)_9]^{3+}$ **(3)**. Ellipsoids are drawn with 50% probability boundaries, and the ethyl groups have been omitted for the sake of clarity. The molecule is on a $\bar{6}$ position and therefore has $C_{3h}$ point group symmetry. The atoms with (′) and (″) labels are related by the $C_3$ axis while the ones with (*) labels are related by the mirror plane.

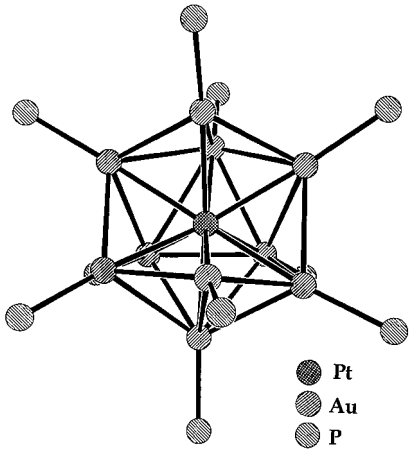


**Figure 5.** A drawing of the approximate coordination core of $[Pt(AuPEt_3)_{10}](BPh_4)_2$ **($2(BPh_4)_2$)**.

lence is in agreement with low-temperature $^{31}P$ NMR data which shows that the nine $PEt_3$ moieties exist in a 2:1 intensity ratio. $^{31}P\{^1H\}$ NMR data also verify that Pt is located in the center of the $PtAu_9$ cluster framework as expected from other Pt−Au clusters and site preference arguments.[1,2,18,24,25]

The metal core geometry of **3** is toroidal in accord with the predictions of cluster-bonding models[2,18,25] and is very similar to the structures reported for the $PPh_3$-stabilized trimetallic clusters $[(AgNO_3)Pt(AuPPh_3)_8](NO_3)_2$ (Figure 1)[19] and $[(CuCl)Pt(AuPPh_3)_8](NO_3)_2$.[22] A comparison of selected bond distances and angles in these clusters is shown in Table 3. The average Pt−Au bond distance in **3** is 2.710 Å and is slightly longer than that in $[(AgNO_3)Pt(AuPPh_3)_8](NO_3)_2$ (2.650 Å) and $[(CuCl)Pt(AuPPh_3)_8](NO_3)_2$ (2.673 Å). The adjacent Au−Au distances of **3** (av 2.856 Å) are similar to those of the trimetallic clusters (av 2.850 and 2.881 Å) and are within the range of those observed in other $PPh_3$-stabilized Pt−Au clusters.[1,21,26] Even though the clusters are stabilized by different phosphines, the trimetallic clusters (av 2.27 and 2.29 Å) and **3** (av 2.30 Å) have very similar Au−P distances. The Pt−Au−P bond angles of the Au1 atoms in the mirror plane are nearly linear (178.9°, av 171.8°, av 173.1°) while the angles with the other Au2 atoms are distinctly bent (156.9°, av 158.0°, av 156.9°) away from the mirror plane. Such deviations from linearity are common for Pt−Au clusters.

**Molecular Structure of $[Pt(AuPEt_3)_{10}](BPh_4)_2$ ($2(BPh_4)_2$).** The structure of **$2(BPh_4)_2$** could not be satisfactorily solved due to unresolved crystallographic problems (see Experimental Section). Nevertheless, an approximate structure of the cluster dication was clearly evident in the refinements and is shown in Figure 5. It is unlikely that the gross structure of the cluster core is incorrect, and it is consistent with analytical and spectroscopic data. Positional and thermal parameters and distances and angles are not reported, however, due to the unsatisfactory solution of the structure. This approximate structure illustrates that the 18-electron cluster **2** has a spheroidal arrangement in accord with the predictions of bonding models.[2,18,25] The cluster core is best described as a fragment of a centered icosahedron with two adjacent vertices vacant. This geometry is very similar to that of the 18-electron, $PtM_{10}$ trimetallic clusters $[Pt(H)(AgNO_3)_2(AuPPh_3)_8](NO_3)$ and $[Pt(H)(CuCl)_2(AuPPh_3)_8](NO_3)$.[6,7]

**$H_2$ Activation by 3. Spectroscopic Analysis.** A $CH_2Cl_2$ solution of **3** immediately changed from dark brown to orange-red upon replacement of a $N_2$ atmosphere with ca. 1 atm of $H_2$. This color change is typical for the 2-electron reduction of a 16-electron Pt−Au cluster.[1,9,27] The original color reappeared within a few minutes after $H_2$ was substituted by an atmosphere of $N_2$. These reversible color changes were readily monitored

(24) Mingos, D. M. P.; Zhenyang, L. *Comments Inorg. Chem.* **1989**, *9*, 95.
(25) Mingos, D. M. P.; Johnson, R. J. *Struct. Bonding* (*Berlin*) **1987**, *68*, 29.
(26) Ito, L. N.; Sweet, J. D.; Mueting, A. M.; Pignolet, L. H.; Schoondergang, M. F. J.; Steggerda, J. J. *Inorg. Chem.* **1989**, *28*, 3696.
(27) Schoondergang, M. F. J. Ph.D. Thesis, University of Nijmegen, The Netherlands, 1992.

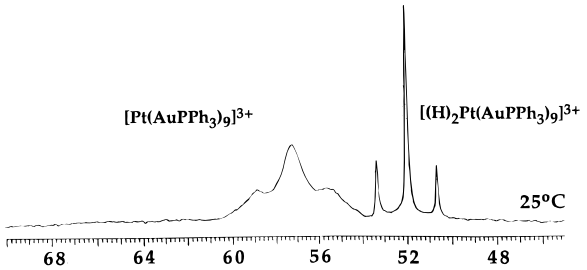


**Figure 6.** $^{31}P\{^1H\}$ NMR spectrum of $[Pt(AuPEt_3)_9]^{3+}$ **(3)** under 1 atm of $H_2$ (121.3 MHz with $CD_2Cl_2$ as solvent).

by UV−vis absorption spectroscopy. Under a $N_2$ atmosphere, four bands were observed: $\lambda = 330$ nm ($\log \epsilon = 4.68$), $\lambda = 344$ nm ($\log \epsilon = 4.59$), $\lambda = 402$ nm ($\log \epsilon = 4.09$), and $\lambda = 420$ nm ($\log \epsilon = 4.16$). Under an atmosphere of $H_2$, three less intense bands were observed: $\lambda = 346$ nm ($\log \epsilon = 4.05$), $\lambda = 378$ nm ($\log \epsilon = 3.80$), and $\lambda = 438$ nm ($\log \epsilon = 4.00$). These changes are similar to those observed with $[Pt(AuPPh_3)_8]^{2+}$.[9] The presence of $H_2$ also produced changes in the $^{31}P$ and $^1H$ NMR spectra of **3** in $CD_2Cl_2$ solution. Under a $N_2$ atmosphere, the room temperature $^{31}P\{^1H\}$ NMR spectrum contained a broad singlet at $\delta = 57.0$ ppm with $^{195}Pt$ satellites ($^2J_{^{195}Pt-P} = 412$ Hz) as previously described and shown in Figure 2. Under a $H_2$ atmosphere, however, the intensity of this resonance decreased, and a new sharp peak appeared at $\delta = 51.8$ ppm with $^{195}Pt$ satellites ($^2J_{^{195}Pt-P} = 320$ Hz) as shown in Figure 6. This 92 Hz decrease of the $^{195}Pt-P$-coupling constant is characteristic of an increase in coordination number and electron count.[1,6−8,28]

Similar changes were observed in the $^1H$ NMR spectra of **3** at 25 °C. Under a $N_2$ atmosphere, the $CD_2Cl_2$ solution spectrum only contained the proton resonances of the $PEt_3$ ligand. Upon substitution of the $N_2$ atmosphere by the $H_2$, a multiplet with phosphorus coupling ($^3J_{^{31}P-H} = 15$ Hz) appeared at 3.24 ppm. The intense ethyl resonances procluded the observation of Pt−H coupling. These changes in the $^{31}P$ and $^1H$ NMR spectra were reversible upon removal of the $H_2$ atmosphere. This result is similar to the well-known reversible $H_2$ addition to $[Pt(AuPPh_3)_8]^{2+}$ to give the dihydride $[(H)_2Pt(AuPPh_3)_8]^{2+}$.[9,10] It is therefore concluded that the 16-electron cluster $[Pt(AuPEt_3)_9]^{3+}$ reversibly adds $H_2$ to form the 18-electron dihydride $[(H)_2Pt(AuPEt_3)_9]^{3+}$ **(6)** as shown in eq 1. The value of $K_{eq}$

$$[Pt(AuPEt_3)_9]^{3+}\ (\mathbf{3}) + H_2 \rightleftarrows [(H)_2Pt(AuPEt_3)_9]^{3+}\ (\mathbf{6}) \quad (1)$$

for the reaction in eq 1 was calculated from the relative $^{31}P$ NMR intensities of **3** and **6** and the measured molar concentration of $H_2$ ($3.9 \times 10^{-3}$ mol $L^-$ at 1 atm) (see Experimental Section). The value obtained was $1.1 \times 10^3$ $M^{-1}$. The equilibrium constant for the reversible binding of $H_2$ by $[Pt(AuPPh_3)_8]^{2+}$ is $8.7 \times 10^3$ $M^{-1}$ under the same conditions of temperature and pressure.[29] The rate of the reversible $H_2$ addition to **3** is slower than for $[Pt(AuPPh_3)_8]^{2+}$. Significant line broadening due to $H_2$ exchange was observed in the 25 °C $^{31}P$ NMR spectrum of $[Pt(AuPPh_3)_8]^{2+}$ under 1 atm of $H_2$ in $CH_2Cl_2$ solution.[9,10,29] In the case of **3**, the peak due to **6** is sharp under identical conditions (Figure 6).

The temperature dependence on the $^{31}P\{^1H\}$ NMR spectrum of **3** under $H_2$ was also studied. As was observed under a $N_2$ atmosphere, lowering of the temperature to −80 °C caused the resonance due to **3** to decoalesce into two triplet patterns as shown in Figure 2. The resonance due to **6** remained sharp at −80 °C. This indicated that the rate of skeletal rearrangement of **6** is greater than that of **3**.

**Table 4.** Turnover Rate Data for Catalytic $H_2-D_2$ Equilibration under Homogeneous Conditions[a]

| compound | turnover rate × $10^2$ ($s^{-1}$) for HD production |
|---|---|
| 16-Electron Compounds | |
| $[Pt(AuPEt_3)_9]^{3+}$ (**3**) | 13. |
| $[Pt(AuPPh_3)_8]^{2+}$ [b] | 7.5 |
| $[Pt(Au(p\text{-}tolyl_3P)_8]^{2+}$ [c] | 22. |
| $[(PPh_3)PtAuPPh_3)_6]^{2+}$ | 2.1 |
| 18-Electron Compounds | |
| $[Pt(CO)(AuPEt_3)_9]^{3+}$ (**6**) | 0.94 |
| $[Pt(CO)(AuPPh_3)_8]^{2+}$ | 0.71 |
| $[Pt(PEt_3)(AuPEt_3)_9]^{3+}$ (**5**) | 0.59 |

[a] Turnover rates were determined as described in ref 10. The experimental error in turnover rate is estimated to be ±5%. Values reported are averages of at least two determinations. Compound concentrations were in the range $(2.5-6.4) \times 10^{-4}$ M with nitrobenzene as solvent, initial $H_2 + D_2$ partial pressure of 760 Torr, and 30 °C. Values for the $PPh_3$-ligated compounds were taken from ref 10.

**Catalytic $H_2-D_2$ Equilibration.** The $H_2-D_2$ equilibration reaction ($H_2 + D_2 \rightleftarrows 2HD$) was used to investigate the catalytic $H_2$ activation abilities of the newly prepared $PEt_3$-ligated clusters. The rate of homogeneous, catalytic HD production from an equimolar mixture of $H_2$ and $D_2$ (1 atm total pressure, nitrobenzene solvent, 30 °C) was experimentally determined using the same procedure and equipment of a previous study.[10] The reader is referred to this study for details of the experiment and for a discussion of the controls that demonstrate the homogeneous, non-diffusion-limited nature of the catalysis. The activities are reported as turnover rates with units of (mol of HD) (mol of cluster)$^{-1}$ $s^{-1}$ and are listed in Table 4. Some representative $PPh_3$-ligated clusters are included in this table for comparison purposes.

## Discussion

The first triethylphosphine-stabilized Pt−Au cluster compounds, $[Pt(AuPEt_3)_{10}]^{2+}$ (**2**) and $[Pt(AuPEt_3)_9]^{3+}$ (**3**), were prepared by the direct reaction of $Pt(PEt_3)_3$ with $AuPEt_3NO_3$ under a dihydrogen atmosphere (Scheme 1). Compound **2** is the highest-nuclearity homoleptic M-centered $[M(AuPR_3)_n]^{x+}$ cluster presently known. The highest-nuclearity homoleptic Pt-centered cluster where $PR_3$ is $PPh_3$ is $[Pt(AuPPh_3)_8]^{2+}$,[30,31] although the hydrido cluster $[Pt(H)(AuPPh_3)_9]^{2+}$ has recently been reported.[15,32] The smaller cone angle of $PEt_3$ (132°)[33] relative to that of $PPh_3$ (145°) sterically allows more $AuPR_3$ units to aggregate about the central Pt atom. This is a well-known phenomenon in gold cluster chemistry. The largest homoleptic $PPh_3$-stabilized gold-centered cluster is $[Au(AuPPh_3)_8]^{3+}$,[34] while the cluster $[Au(AuPR_3)_{10}]^{3+}$ forms with the sterically smaller ligands $PMe_2Ph$ and $PMePh_2$.[35,36]

(28) Bour, J. J.; van den Berg, W.; Schlebos, P. P. J.; Kanters, P. P. J.; Schoondergang, M. F. J.; Bosman, W. P.; Smits, J. M. M.; Beurskens, P. T.; Steggerda, J. J.; van der Sluis, P. *Inorg. Chem.* **1990**, *29*, 2971.
(29) Fanning, B. D.; Pignolet, L. H., to be submitted for publication.
(30) Bour, J. J.; Kanters, R. P. F.; Schlebos, P. P. J.; Bosman, W. P.; Behm, H.; Beurskens, P. T.; Steggerda, J. J. *Recl. Trav. Chim. Pays-Bas* **1987**, *106*, 157.
(31) Bour, J. J.; Kanters, R. P. F.; Schlebos, P. P. J.; Steggerda, J. J. *Recl. Trav. Chim. Pays-Bas* **1988**, *107*, 211.
(32) Roush, W. *Science* **1996**, *271*, 1060.
(33) Tolman, C. A. *Chem. Rev.* **1977**, *77*, 313.
(34) Steggerda, J. J.; Bour, J. J.; van der Velden, J. W. A. *Recl. Trav. Chim. Pays-Bas* **1982**, *101*, 164.
(35) Hall, K. P.; Gilmour, D. I.; Mingos, D. M. P. *J. Organomet. Chem.* **1984**, *268*, 275.
(36) Copley, R. C. B.; Mingos, D. M. P. *J. Chem. Soc., Dalton Trans.* **1996**, 479.

The reactivity and structures of these clusters are in agreement with the electron-counting formalism of Mingos and Stone described above.[2,16,18] The 18-electron cluster **2** was converted into the 16-electron cluster **3** by *oxidation* with 2 equiv of ferricinium ion $Fc^+$. Cluster **3** was converted into **2** by *reduction* with $H_2$ in the presence of $[AuPEt_3]^+$. Cluster **3** was also observed to cleanly add the 2-electron donors CO and $PEt_3$ to form the 18-electron clusters $[(CO)Pt(AuPEt_3)_9]^{3+}$ (**4**) and $[(PEt_3)Pt(AuPEt_3)_9]^{3+}$ (**5**), respectively. Cluster **2** was unreactive toward these substrates in agreement with its closed shell 18-electron configuration. Single crystal X-ray diffraction results show that **2** has a spheroidal geometry best described as a Pt-centered icosahedral fragment (Figure 5). This type of structure is typical of 18-electron clusters.[1−3] X-ray results also show that **3** has a flattened, toroidal structure in which the $PtAu_9$ framework has a centered, tricapped trigonal prismatic geometry (Figure 4). This structure is similar to those reported for the $PPh_3$-ligated, 16-electron clusters $[(AgNO_3)Pt(AuPPh_3)_8](NO_3)_2$ (Figure 1)[19] and $[(CuCl)Pt(AuPPh_3)_8](NO_3)_2$.[22]

Cluster **3** exhibited a broad resonance in the room temperature $^{31}P\{^1H\}$ NMR spectrum indicative of a dynamic rearrangement process. Lowering the temperature to about −80 °C resulted in a frozen-out spectrum that consisted of two resonances in a 2:1 intensity ratio as shown in Figure 3. This 2:1 pattern is consistent with the tricapped trigonal prismatic geometry found in the solid state. A very similar behavior was reported with $[(AgNO_3)Pt(AuPPh_3)_8]^{2+}$.[37] The Cu analog $[(CuCl)Pt(AuPPh_3)_8]^{2+}$ also shows a broadened $^{31}P$ NMR resonance at room temperature indicating exchange broadening, but low-temperature spectra were not reported.[22] The fact that the dynamic rearrangement process can be frozen out at −80 °C for **3** and $[(AgNO_3)Pt(AuPPh_3)_8]^{2+}$ is unusual. Most Pt−Au clusters exhibit sharp signals in their $^{31}P$ NMR spectra even at low temperature due to rapid skeletal rearrangement.[1−3,15,37] The significantly slower rearrangement rate observed in the above $PtM_9$ clusters may be due to their stable tricapped, trigonal prismatic structures.

Compound **3**, like $[Pt(AuPPh_3)_8]^{2+}$, was found to reversibly add $H_2$ in solution to form a dihydride cluster as shown in eq 1. This was directly observed by $^{31}P\{^1H\}$ and $^1H$ NMR (Figure 6). The dihydride formulation is based on the similarity to the thoroughly studied $[(H)_2Pt(AuPPh_3)_8]^{2+}$ system.[9,10,29] The equilibrium constant for the formation of $[(H)_2Pt(AuPEt_3)_9]^{3+}$ (**6**) (eq 1) was found to be $1.1 \times 10^3$ $M^{-1}$ ($CD_2Cl_2$ solution, 25 °C). This value is smaller than the value ($8.7 \times 10^3$ $M^{-1}$) determined for the formation of $[(H)_2Pt(AuPPh_3)_8]^{2+}$ under identical conditions.[29] This small difference is probably the result of lower electron density on the metal core of $[Pt(AuPEt_3)_9]^{3+}$ compared with that on $[Pt(AuPPh_3)_8]^{2+}$. The higher positive charge on the former must account for this even though the $PEt_3$ ligand is more basic than $PPh_3$. This is also consistent with the higher CO stretching frequency observed for $[(CO)Pt(AuPEt_3)_9]^{3+}$ (1948 $cm^{-1}$) compared to that of $[(CO)Pt(AuPPh_3)_8]^{2+}$ (1940 $cm^{-1}$).[21] In agreement with the above electron density arguments, it was observed previously that the cluster ligated with the more basic tri-*p*-tolylphosphine, $\{Pt[Au(p\text{-tolyl})_3P]_8\}^{2+}$, favors the addition of $H_2$ compared with the $PPh_3$ analog.[10]

The rate of reversible $H_2$ addition to **3** (eq 1) is slower than that with $[Pt(AuPPh_3)_8]^{2+}$. This was determined qualitatively by $^{31}P$ NMR. The spectrum of **3** under 1 atm of $H_2$ ($CH_2Cl_2$ solvent, 25 °C) showed a sharp resonance due to the dihydride cluster in addition to a resonance of unreacted **3** (Figure 6). An identical experiment with $[Pt(AuPPh_3)_8]^{2+}$ showed significant broadening (near coalescence) of signals due to $[Pt(AuPPh_3)_8]^{2+}$ and $[(H)_2Pt(AuPPh_3)_8]^{2+}$ (see Figure 6 of ref 10). Since the chemical shift differences between the parent clusters and their dihydrides are similar, the rate of $H_2$ exchange is significantly faster with the $[Pt(AuPPh_3)_8]^{2+}$ system. The only explanation we can put forth for this is the special stability of the tricapped, trigonal prismatic geometry of the $PtAu_9$ clusters noted above (Figures 1 and 4). Recall that these clusters also underwent skeletal rearrangement at much slower rates than other Pt−Au clusters.

Cluster **3** is an excellent homogeneous catalyst for $H_2-D_2$ equilibration as shown in Table 4. It is apparent from the data in this table that the $PEt_3$-containing clusters give similar rates and follow the same general trends observed with $PPh_3$-ligated clusters.[10,11] The 16-electron clusters give significantly larger turnover rates than the 18-electron clusters. Among the 16-electron clusters, **3** was more active than the $PPh_3$-containing clusters $[Pt(AuPPh_3)_8]^{2+}$ and $[(PPh_3)Pt(AuPPh_3)_6]^{2+}$, but less active than the tri-*p*-tolylphosphine derivative $[Pt(Au(p\text{-tolyl}_3P)_8]^{2+}$. Although it might be expected that the 18-electron clusters should be inactive (no $H_2$ binding observed), the low activity is probably due to some dissociation of the ligand which is directly bound to Pt. Such dissociation has not been observed by spectroscopy during catalysis runs, but it is implicated with the CO adducts by kinetic experiments.[10] The initial activity of the 18-electron clusters $[(CO)Pt(AuPEt_3)_9]^{3+}$ and $[(CO)Pt(AuPPh_3)_8]^{2+}$ is zero after the reaction mixture is purged with CO and subjected to several freeze−pump−thaw cycles. The activity gradually increases with time suggesting that CO is being lost to give some of the 16-electron cluster.

The mechanism for $H_2-D_2$ equilibration has been extensively studied for several $PPh_3$-ligated clusters.[10,15] From $PPh_3$ rate inhibition studies, a key step in the mechanism is reversible $PPh_3$ dissociation from the 18-electron dihydride giving an intermediate with a vacant gold site. The proposed mechanism for $[Pt(AuPPh_3)_8]^{2+}$ is shown in eq 2 where MP represents the starting cluster $[Pt(AuPPh_3)_8]^{2+}$.[10,15] The rates of the phosphine

$$MP \underset{-H_2}{\overset{H_2}{\rightleftharpoons}} H_2MP \underset{P}{\overset{-P}{\rightleftharpoons}} H_2M \underset{-HD}{\overset{D_2}{\rightleftharpoons}} H_2D_2M \qquad (2)$$

dissociation and $D_2$ addition steps are both kinetically important. Therefore, it is difficult to draw simple conclusions about the relative rates for clusters with different phosphine ligands, number of $AuPR_3$ groups, and charges. The primary conclusion which may be drawn from this study is that the catalytic behavior of the $PEt_3$-ligated Pt−Au clusters is similar to that of the $PPh_3$ compounds. The new $PEt_3$-ligated clusters prepared in this paper should therefore be useful in our efforts to study the catalytic properties of supported Pt−Au clusters.[12] The increased volatility of $PEt_3$ compared with that of $PPh_3$ should also make these clusters good precursors for heterogenized Pt−Au particle catalysts.[1,14,38]

## Experimental Section

**Measurements and Reagents.** Elemental analyses were carried out by Guelph Chemical Laboratories, Ltd., Guelph, Ontario, Canada. Fast atom bomdardment mass spectroscopy (FABMS) experiments were carried out with the use of a VG Analytical, Ltd., 7070E-HF high-resolution double-focusing mass spectrometer equipped with a VG 11/250 data system. IR spectra were measured in CsI pellets on a Perkin-Elmer 1710 FT-IR spectrometer. Conductivity measurements were made with use of a Yellow Springs Model 35 conductance meter. Ultraviolet and visible spectra were obtained on a Hewlett Packard

(37) Kanters, R. P. F. Ph.D. Thesis, University of Nijmegen, The Netherlands, 1990.

(38) Schwank, J. *Gold Bull.* **1985**, *18*, 1.

8452A diode array spectrophotometer. $^{31}$P NMR spectra were recorded at 121.5 MHz with use of a Varian VXR-300 MHz spectrometer and at 202.5 MHz with use of a Varian VXR-500 MHz spectrometer. $^{1}$H NMR spectra were recorded at 300 MHz and $^{13}$C NMR spectra were recorded at 75.5 MHz with use of a Varian VXR-300 MHz spectrometer. The $^{31}$P and $^{13}$C NMR spectra were run with proton decoupling, and $^{31}$P NMR spectra are reported in ppm relative to an internal standard trimethyl phosphate (TMP), with positive shifts downfield. $^{13}$C NMR spectra are reported in ppm relative to external standard tetramethylsilane (TMS), with positive shifts downfield. Solvents were distilled and dried prior to use. $PEt_3$ was obtained from Aldrich and used without further purification. $Pt(PEt_3)_3$ and $AuPEt_3Cl$ were prepared as described in the literature.[39,40] All manipulations were carried out under a purified $N_2$ atmosphere with use of standard Schlenk techniques unless otherwise noted. This airless procedure was used even though the final clusters are stable to air and moisture.

**Preparation of Complexes. $AuPEt_3NO_3$ (1)**. A sample of 1.000 g (2.85 mmol) of $AuPEt_3Cl$ was dissolved in 30 mL of $CH_2Cl_2$. This solution was added dropwise over a 30 min period to a foil-wrapped flask at 0 °C which contained 0.485 g (2.85 mmol) of $AgNO_3$ dissolved in 50 mL of MeOH. After the solution was stirred for 1 h at 0 °C, the reaction was filtered through diatomaceous earth, and the filtrate was evaporated to dryness at 0 °C. The white residue was redissolved in 30 mL of $CH_2Cl_2$ and filtered through diatomaceous earth. The filtrate was again evaporated to dryness at 0 °C. The white residue was dissolved in a minimal amount of acetone and layered with hexanes. After 24 h at 0 °C, white needles were isolated by filtering off the mother liquor, washing with cold hexanes, and drying in vacuo. Yield: 1.953 g (5.18 mmol), 93% calculated for Au. Anal. Calcd for $AuPC_6H_{15}NO_3$ ($M_r$ 377.16): C, 19.11; H, 4.02; N, 3.71. Found: C, 19.12; H, 4.02; N, 3.73. IR: $\nu$(coordinated $NO_3$) 1497, 1488, 1478, 1272 cm$^{-1}$. $^{31}$P NMR (acetone, 20 °C): $\delta$ 26.7 (s).

**$[Pt(AuPEt_3)_{10}](PF_6)_2$ ($2(PF_6)_2$) and $[Pt(AuPEt_3)_9](PF_6)_3$ ($3(PF_6)_3$). Method A.** A 72.5 mg (0.132 mmol) sample of $Pt(PEt_3)_3$ was dissolved in 50 mL of THF, and $H_2$ was bubbled through the solution for 15 min. Over a 5 min period, the resulting light yellow solution was added to 500 mg (1.33 mmol) of solid **1** under a $H_2$ atmosphere. $H_2$ was bubbled through the resulting burgundy solution for 2 h at room temperature, and a red-orange solid began to precipitate. After the solution was stirred under $H_2$ overnight, the solution was concentrated by evaporation to 20 mL. The orange-red precipitate was filtered off and redissolved in 20 mL of MeOH. A saturated solution of $KPF_6$ in MeOH was added dropwise to the bright orange solution until an orange solid of $\mathbf{2(PF_6)_2}$ precipitated. The precipitate of $\mathbf{2(PF_6)_2}$ was filtered off, recrystallized by slow diffusion of MeOH into an acetone solution of the product, and dried in vacuo. Yield: 325 mg (0.0894 mmol), 67.8% calculated for Pt. The filtrate from the above reaction was concentrated by evaporation until a deep red-brown oil formed. The red oil was dissolved in 10 mL of MeOH, and a saturated MeOH solution of $KPF_6$ was added until a brown solid of $\mathbf{3(PF_6)_3}$ precipitated. The precipitate of $\mathbf{3(PF_6)_3}$ was collected on a frit and washed with MeOH. A crystal suitable for X-ray diffraction was obtained by slow diffusion of MeOH into an acetone solution of $\mathbf{3(PF_6)_3}$. Yield: 124 mg (0.0358 mmol), 27.1% calculated for Pt. Analytical data for $\mathbf{2(PF_6)_2}$ and $\mathbf{3(PF_6)_3}$ are listed after each alternative preparation below.

**$[Pt(AuPEt_3)_{10}](PF_6)_2$ ($2(PF_6)_2$). Method B.** A 100 mL Schlenk flask equipped with a Teflon stir bar was charged with 100 mg (0.0289 mmol) of $\mathbf{3(PF_6)_3}$ and 21.8 mg (0.0577 mmol) of **1** and placed under a $H_2$ atmosphere. The reagents were dissolved in 30 mL of $H_2$-saturated THF to form a reddish-brown solution. With $H_2$ bubbling through it, the solution color changed to a deep burgundy, and an orange solid precipitated after 2 h. After the solution was stirred under a $H_2$ atmosphere overnight, the orange-red precipitate was collected on a frit, recrystallized by slow diffusion of MeOH into an acetone solution of the product, and dried in vacuo. Yield: 65.7 mg (0.0181 mmol), 62.5% calculated for Pt. Anal. Calcd for $PtAu_{10}P_{12}C_{60}H_{150}F_{12}$ ($M_r$ 3636.52): C, 19.82; H, 4.17; P, 10.22. Found: C, 19.84; H, 3.96; P, 10.27. IR: $\nu(PF_6)$ 840 cm$^{-1}$. $^{31}$P NMR (acetone, 20 °C): $\delta$ 51.4 (s with $^{195}$Pt satellites, $^{2}J_{^{195}Pt-P} = 354$ Hz), $\delta$ −146.4 (sept, $^{1}J_{^{19}F-P} = 699$ Hz) due to $PF_6^-$. The equivalent conductance (175.2 cm$^2$ mhos mol$^{-1}$) is indicative of a 2:1 electrolyte in $CH_3CN$ solution. FABMS (*m*-nitrobenzyl alcohol matrix): observed *m/z* 3636.6 {calcd 3636.5 for $[Pt(AuPEt_3)_{10}(PF_6)_2]^+ = M^+$}, 3518.7 {calcd 3518.3 for [M less $PEt_3$]$^+$}, 3373.7 {calcd 3373.4 for [M less ($PEt_3$, $PF_6$)]$^+$}, 3176.1 {calcd 3176.4 for [M less ($AuPEt_3$, $PF_6$)]$^+$}, 3058.3 {calcd 3058.2 for [M less ($AuPEt_3$, $PF_6$, $PEt_3$)]$^+$}, 2940.5 {calcd 2940.1 for [M less ($AuPEt_3$, $2PEt_3$, $PF_6$)]$^+$}.

**$[Pt(AuPEt_3)_9](PF_6)_3$ ($3(PF_6)_3$). Method B.** A 75.1 mg (0.137 mmol) sample of $Pt(PEt_3)_3$ was dissolved in 50 mL of EtOH, and $H_2$ was bubbled through the solution for 15 min. Over a 5 min period, the resulting light yellow solution was added to 0.465 g (1.23 mmol) of solid **1**. Immediately after this, 200 mg of solid $KPF_6$ (1.23 mmol) was added to the brownish-red solution. $H_2$ was bubbled through the solution for 2 h at room temperature, and a brown solid began to precipitate. After the solution was under a $H_2$ atmosphere for 6 h, the solid was filtered off and recrystallized by slow diffusion of EtOH into an acetone solution of the product. Yield: 392 mg (0.113 mmol), 82.5% calculated for Pt. Anal. Calcd for $PtAu_9P_{12}C_{54}H_{135}F_{12}$ ($M_r$ 3466.34): C, 18.71; H, 3.93; P, 10.72. Found: C, 18.69; H, 3.79; P, 10.48. IR: $\nu(PF_6)$ 840 cm$^{-1}$. $^{31}$P NMR (acetone, 20 °C): $\delta$ 57.0 (s with $^{195}$Pt satellites, $^{2}J_{^{195}Pt-P} = 412$ Hz), $\delta$ −146.4 (sept, $^{1}J_{^{19}F-P} = 706$ Hz) due to $PF_6^-$. The equivalent conductance (231.4 cm$^2$ mhos mol$^{-1}$) is indicative of a 3:1 electrolyte in $CH_3CN$ solution. FABMS (*m*-nitrobenzyl alcohol matrix): observed *m/z* 3321.0 {calcd 3321.2 for $[Pt(AuPEt_3)_9(PF_6)_2]^+ = M^+$}, 3176.0 {calcd 3176.2 for [M less $PF_6$]$^+$}, 3057.8 {calcd 3058.0 for [M less ($PEt_3$, $PF_6$)]$^+$}, 2742.7 {calcd 2742.9 for [M less ($AuPEt_3$, $PEt_3$, $PF_6$)]$^+$}. UV−vis ($CH_2Cl_2$) [$\lambda_{max}$, nm (log $\epsilon_{max}$)]: 330 (4.68), 344 (4.59), 402 (4.09), 420 (4.16).

**$[Pt(AuPEt_3)_{10}](BPh_4)_2$ ($2(BPh_4)_2$).** A 50.0 mg (0.0137 mmol) sample of $\mathbf{2(PF_6)_2}$ was dissolved in 5 mL of acetone. A methanol solution (2 mL) of $NaBPh_4$ (46.9 mg, 0.137 mmol) was added to the stirred solution. A bright orange precipitate immediately formed. After the solution was stirred for 10 min, the solid was collected on a frit and washed with 1 mL of methanol and 10 mL of diethyl ether. Yield: 53.4 mg (0.0134 mmol), 97.8% calculated for Pt. Anal. Calcd for $PtAu_{10}P_{10}C_{108}H_{190}B_2$ ($M_r$ 3985.08): C, 32.55; H, 4.82; P, 7.77. Found: C, 32.73; H, 4.89; P, 7.84. The equivalent conductance (186.1 cm$^2$ mhos mol$^{-1}$) is indicative of a 2:1 electrolyte in $CH_3CN$ solution. The $^{31}$P NMR spectrum in the $PEt_3$ region was identical to that of the $PF_6$ salt. X-ray quality crystals of $\mathbf{2(BPh_4)_2}$ were prepared as follows. An acetone solution of $\mathbf{2(PF_6)_2}$ (30 mg in 0.5 mL) was layered with a saturated solution of $NaBPh_4$. Overnight, large red crystals had grown at the solvent interface.

**$[(CO)Pt(AuPEt_3)_9](PF_6)_3$ ($4(PF_6)_3$).** A 100 mg (0.0289 mmol) sample of $\mathbf{3(PF_6)_3}$ was dissolved in 10 mL of acetone. CO was bubbled through the brown solution for 10 min. The color of the solution immediately changed to bright orange. The solvent was removed in vacuo. The orange residue was recrystallized by slow diffusion of diethyl ether into an acetone solution of the product. Yield: 96.7 mg (0.0277 mmol), 95.9% calculated for Pt. Isotopically labeled [($^{13}$CO)-$Pt(AuPEt_3)_9](PF_6)_3$ was prepared by the same procedure using $^{13}$CO gas. Anal. Calcd for $PtAu_9P_{12}C_{55}H_{135}F_{12}O$ ($M_r$ 3494.35): C, 18.90; H, 3.90; P, 10.63. Found: C, 18.88; H, 3.87; P, 10.57. IR: $\nu(PF_6)$ 840 cm$^{-1}$; $\nu$(CO) 1948 cm$^{-1}$, $\nu$($^{13}$CO) 1904 cm$^{-1}$. $^{31}$P NMR (acetone, 20 °C): $\delta$ 51.2 (s with $^{195}$Pt satellites, $^{2}J_{^{195}Pt-P} = 338$ Hz), $\delta$ −146.2 (sept, $^{1}J_{^{19}F-P} = 707$ Hz) due to $PF_6^-$. $^{13}$C NMR (acetone, 20 °C): $^{13}$-CO $\delta$ 209.8 (m) with $^{1}J_{^{195}Pt-C} = 1178$ Hz and $^{3}J_{^{31}P-C} = 10$ Hz. The equivalent conductance (234.7 cm$^2$ mhos mol$^{-1}$) is indicative of a 3:1 electrolyte in $CH_3CN$ solution. FABMS (*m*-nitrobenzyl alcohol matrix): observed *m/z* 3349.6 {calcd 3349.2 for $[(CO)Pt(AuPEt_3)_9(PF_6)_2]^+ = M^+$}, 3321.5 {calcd 3321.2 for [M less CO]$^+$}, 3176.4 {calcd 3176.2 for [M less (CO, $PF_6$)]$^+$}, 3058.4 {calcd 3058.1 for [M less (CO, $PF_6$, $PEt_3$)]$^+$}, 2743.2 {calcd 2742.9 for [M less (CO, $PF_6$, $PEt_3$, $AuPEt_3$)]$^+$}.

**$[(PEt_3)Pt(AuPEt_3)_9](PF_6)_3$ ($5(PF_6)_3$).** A 98.5 mg (0.0289 mmol) sample of $\mathbf{3(PF_6)_3}$ was dissolved in 10 mL of acetone. Via syringe, 1.0 mL of a $2.84 \times 10^{-2}$ M $PEt_3$ solution (0.42 mL in 100.0 mL of $CH_2Cl_2$) was added dropwise to the stirred, brown solution. The color of the reaction immediately changed to bright orange. After being stirred for 1.5 h, 10 mL of hexanes was added to precipitate an orange

(39) Yoshida, T.; Matsuda, T.; Otsuka, S. *Inorg. Synth.* **1990**, *28*, 120.
(40) Al-Saady, A. K.; McAuliffe, C. A.; Parish, R. V.; Sandbank, J. A. *Inorg. Synth.* **1985**, *23*, 191.

solid. The orange precipitate was recrystallized by slow diffusion of diethyl ether into an acetone solution of the product. Anal. Calcd for $PtAu_9P_{13}C_{60}H_{150}F_{12}$ ($M_r$ 3584.52): C, 20.10; H, 4.27; P, 11.23. Found: C, 20.11; H, 4.23; P, 11.21. IR: $\nu(PF_6)$ 839 $cm^{-1}$. $^{31}P$ NMR (acetone, 20 °C): $\delta$ 49.8 (int = 9, d, $^3J_{P-P}$ = 30 with $^{195}Pt$ satellites, $^2J_{^{195}Pt-P}$ = 386 Hz), $\delta$ 62.2 (int = 1, m, $^3J_{P-P}$ = 30 Hz with $^{195}Pt$ satellites, $^1J_{^{195}Pt-P}$ = 2356 Hz), $\delta$ −146.3 (sept, $^1J_{^{19}F-P}$ = 706 Hz) due to $PF_6^-$. The equivalent conductance (229.2 $cm^2$ mhos $mol^{-1}$) is indicative of a 3:1 electrolyte in $CH_3CN$ solution. FABMS (*m*-nitrobenzyl alcohol matrix): 3439.1 {calcd 3439.4 for $[(PEt_3)Pt(AuPEt_3)_9(PF_6)_2]^+ = M^+$}, 3320.8 {calcd 3321.2 for [M less $PEt_3$]$^+$}, 3175.7 {calcd 3176.2 for [M less ($PEt_3$, $PF_6$)]$^+$}, 3057.7 {calcd 3058.1 for [M less (2$PEt_3$, $PF_6$)]$^+$}, 2939.6 {calcd 2939.9 for [M less (3$PEt_3$, $PF_6$)]$^+$}.

**$[(H)_2Pt(AuPEt_3)_9](PF_6)_3$ (6($PF_6$)$_3$).** A 50.1 mg (0.0144 mmol) sample of **3($PF_6$)$_3$** was dissolved in 10 mL of acetone. The color changed from red-brown to red-orange after substitution of the $N_2$ atmosphere by $H_2$. Upon replacement of the $H_2$ atmosphere with $N_2$, the original color reappeared. The quantitative reversibility of the $H_2$ addition was confirmed by NMR and UV−vis spectroscopies. $^{31}P$ NMR (acetone, under 1 atm of $H_2$, 20 °C): $\delta$ 51.8 (s with $^{195}Pt$ satellites, $^2J_{^{195}Pt-P}$ = 320 Hz); $\delta$ −146.4 (sept, $^1J_{^{19}F-P}$ = 697 Hz) due to $PF_6^-$. $^1H$ NMR (acetone, under 1 atm of $H_2$, 20 °C): $\delta$ 3.24 (m, $^3J_{^{31}P-H}$ = 15.0 Hz). Pt−H coupling was not observed due to interference from the large ethyl resonances. UV−vis ($CH_2Cl_2$, under 1 atm of $H_2$) [$\lambda_{max}$, nm (log $\epsilon_{max}$)]: 346 (4.05), 378 (3.80), 438 (4.00). The hydrogen adduct was not isolated in the solid state.

**Reaction of 2($PF_6$)$_2$ with $[Fe(\eta^5\text{-}C_5H_5)_2]PF_6$.** A 25.0 mg (0.006 87 mmol) sample of **2($PF_6$)$_2$** was dissolved in 5 mL of acetone. An acetone solution of $[Fe(\eta^5\text{-}C_5H_5)_2]PF_6$ [4.6 mg (0.0139 mmol) in 10 mL] was added dropwise to the stirred reaction over a 15 min period. During this time, the color changed from bright orange to deep red-brown. $^{31}P$ NMR spectroscopy of the reaction mixture showed about 80% conversion to **3($PF_6$)$_3$**, with formation of $[Au(PEt_3)_2]^+$ and other unidentified $PEt_3$ containing byproducts.

**Attempted Reactions of 2($PF_6$)$_2$ with $AgNO_3$ and CuCl.** In separate experiments, solid samples of $AgNO_3$ and CuCl were added to acetone solutions of **2($PF_6$)$_2$.** After the solutions were stirred under a $N_2$ atmosphere for several days, no reaction was observed by $^{31}P$ NMR spectroscopy for either case.

**Attempted Reactions of 3($PF_6$)$_3$ with $AgNO_3$ and CuCl.** In separate experiments, solid samples of $AgNO_3$ and CuCl were added to acetone solutions of **3($PF_6$)$_3$.** Addition of each metal salt immediately produced a color change from dark brown to orange-red. Within minutes, a muddy, deep brown slurry was formed in each solution and metal was observed to form a mirror on the reaction flask. $^{31}P$ NMR of the resultant solutions indicated the presence of a large amount of $[Au(PEt_3)_2]^+$ and other unidentified gold cluster compounds.

**X-ray Structure Determination of $[Pt(AuPEt_3)_9](PF_6)_3$ (3($PF_6$)$_3$). Collection and Reduction of Data.** A summary of crystal data for **3($PF_6$)$_3$** is presented in Table 1. The crystal selected for data collection was mounted in a glass capillary. All data for **3($PF_6$)$_3$** were collected with use of an Enraf-Nonius CAD-4 diffractometer with monochromated Mo K$\alpha$ radiation ($\lambda$ = 0.710 69 Å). A total of 7818 reflections were collected. Of these, 2523 were unique ($R_{int}$ = 0.117); equivalent reflections were merged, and 1489 were considered as observed with $I > 2.0\sigma(I)$. The crystal class and space group for **3($PF_6$)$_3$** was determined by the Enraf-Nonius CAD-4 peak search, centering, and indexing program.[41] The intensities of three representative reflections, which were measured after every 60 min of X-ray exposure time, remained constant throughout data collection indicating crystal and electronic stability. The data were corrected for Lorentz, polarization, and background effects. An empirical absorption correction was applied using the program DIFABS.[42] All calculations were performed using the TEXSAN crystallographic software package of the Molecular Structure Corporation.[43]

**Solution and Refinement of the Structure.** The structure of **3($PF_6$)$_3$** was solved by direct methods.[44,45] The Au, Pt, and P atoms of the cluster cation were refined anisotropically, while all other non-hydrogen atoms were refined isotropically. Hydrogen atoms were not included in the structure refinement. Some residual electron density of ca. 1.6 $e^-$ $Å^{-3}$ was found near the 1, 0, 1/2 position. Attempted modeling of these peaks as methanol or acetone solvent failed. These peaks were probably due to partially occupied, disordered solvent and were not included in the refinement. Positional and thermal parameters for the atoms in the cluster cation are shown in the Supporting Information. An ORTEP representation of the cluster core is shown in Figure 4. A labeling scheme and a drawing of the complete cluster is presented in Figure S1 of Supporting Information. The cluster molecule is on a $\bar{6}$ ($C_{3h}$) position with approximate $\bar{6}m2$ ($D_{3h}$) symmetry. Neutral atom-scattering factors were taken from Cromer and Waber.[46] Anomalous dispersion effects were included in $F_{calc}$ (12), and the values of $\Delta F'$ and $\Delta F''$ were those of Cromer.[47,48]

**Unit Cell Determination of $[Pt(AuPEt_3)_{10}](BPh_4)_2$(2 ($BPh_4$)$_2$).** A red crystal of **2($BPh_4$)$_2$** was attached to a glass fiber with a viscous oil and quickly mounted on the Siemens CCD SMART system for data collection at 173 K.[49] Data were collected in the primitive, metrically orthorhombic cell where $a$ = 19.173 Å, $b$ = 26.603 Å, $c$ = 54.730 Å, and $\alpha = \beta = \gamma = 90°$. This appears to be a superstructure of a C-centered monoclinic cell where $a$ = 26.603 Å, $b$ = 27.372 Å, $c$ = 19.173 Å, and $\beta$ = 90.07°, but there was also the possibility of twinning due to $\beta$ being very close to 90°. Solution and refinement was attempted in the space group $P\bar{1}$ due to problems of pseudo-symmetry in the higher symmetry space groups. Although one complete $[Pt(AuPEt_3)_{10}]^{2+}$ unit clearly appeared in the refinement, the remaining cluster was found on inversion centers making the structure insolvable. Figure 5 provides a drawing of the core of one $[Pt(AuPEt_3)_{10}]^{2+}$ unit as observed in the refinement. We were unable to further refine this structure due to pseudo-symmetry and likely twinning. The structure shown in Figure 5 is consistent with the analytical and spectroscopic data of the cluster (vide infra), but should not be taken as a solved crystal structure. It is only a qualitative representation of what appeared in the partial solution and refinement of the X-ray data as described above. We include it only because it did result unbiased from the X-ray data and provides useful information that helps us understand the nature of the compound.

**NMR Sample Preparation.** NMR samples for the determination of thermodynamic parameters for the reversible binding of $H_2$ to **3** were prepared by transferring 0.500 mL of a $CD_2Cl_2$ solution of known cluster concentration into an NMR tube equipped with a screw valve obtained from J. Young Scientific Glassware. (distributed by Brunfeldt Co., Bartlesville, OK). The solution was freeze−pump−thawed and warmed to room temperature in vacuo. $H_2$ was then added to the head space above the solution to give a total pressure of 760 Torr plus the solvent vapor pressure at that temperature. This procedure was repeated three times. The NMR tube was then sealed with the J. Young valve and shaken for 3 min to enhance the gas−solution equilibration. The vapor pressure of $CD_2Cl_2$ was determined by allowing the apparatus to equilibrate without the addition of $H_2$. The pressures were determined with the use of a diaphram manometer to ±0.1 Torr.

**Thermodynamic Modeling of Reversible $H_2$ Binding to 3.** An equilibrium constant for the reversible addition of $H_2$ to **3** ($K = [\mathbf{3H_2}]/[\mathbf{3}][H_2]$) in $CD_2Cl_2$ at 25 °C was determined from the relative intensities

(41) Schagen, J. D.; Straver, L.; van Meurs, F.; Williams, G. Enraf-Nonius CAD-4; Enraf-Nonius Delft, Scientific Instruments Division, Delft, The Netherlands, 1988.
(42) Walker, N.; Stuart, D. *Acta Crystallogr.* **1983**, *A39*, 158.
(43) All calculations were carried out with use of the Molecular Structure Corporations TEXSAN-TEXRAY Structure Analysis Package, version 2.1, 1985.
(44) MITHRIL (an integrated direct methods computer program; University of Glascow, Scotland): Gilmore, C. J. *J. Appl. Crystallogr.* **1984**, *17*, 42.
(45) DIRDIF (Direct Methods for Difference Structures, an automatic procedure for phase extension and refinement of difference structure factors): Beurskens, P. T. Technical Report 1984/1; Crystallography Laboratory, Toernooiveld, 6525 ED Nijmegen, The Netherlands.
(46) Cromer, D. T.; Waber, J. T. *International Tables for X-Ray Crystallography*; Kynoch: Birmingham, England, 1974; Vol. IV, Table 2.2 A.
(47) Cromer, D. T. *International Tables for X-Ray Crystallography*; Kynoch: Birmingham, England, 1974; Vol. IV, Table 2.3.1.
(48) Ibers, J. A.; Hamilton, W. C. *Acta Crystallogr.* **1964**, *17*, 781.
(49) SHELXTL-Plus version 5.0, Siemens Industrial Automation, Inc.: Madison, WI.

of $^{31}P\{^{1}H\}$ NMR peaks due to **3H₂** and **3**, the known concentration of total cluster, and the experimentally determined concentration of dissolved $H_2$. NMR peak intensities were determined with use of the curve-fitting program from the Varian software. The concentration of dissolved $H_2$ was measured under the same conditions of temperature and pressure by comparison of the integrated area of the $^{1}H$ NMR signal of dissolved $H_2$ relative to that of a known concentration of added 1,2-dichloroethane. The concentration of 1,2-dichloroethane was adjusted to give signals of similar area. The value determined for the $H_2$ solubility at 25 °C and 760 Torr total pressure was $3.91 \times 10^{-3}$ M. See details above for NMR sample preparation. This procedure is the same as used previously for analysis of the reversible $H_2$ addition to $[Pt(AuPPh_3)_8]^{2+}$, and the experimental procedure is described in more detail in that paper.[10]

**Acknowledgment.** This work was supported by grants from the National Science Foundation (Grant CHE-9222411) and the University of Minnesota Graduate School. We acknowledge Prof. Doyle Britton and Dr. Victor J. Young, Jr., and the University of Minnesota X-Ray Crystallographic Laboratory for the X-ray structural determination.

**Supporting Information Available:** Tables of data collection and refinement details, all atom parameters, bond lengths, bond angles, anisotropic thermal parameters, and a thermal ellipsoid drawings of the complete molecule (13 pages). Ordering information is given on any current masthead page.

IC960586J